



The influence of water and LPO on the initiation and evolution of mantle shear zones



Philip Skemer^{a,*}, Jessica M. Warren^b, Lars N. Hansen^b, Greg Hirth^c, Peter B. Kelemen^d

^a Department of Earth and Planetary Sciences, Washington University in Saint Louis, 1 Brookings Drive, Saint Louis, MO 63130, USA

^b Department of Geological and Environmental Sciences, Stanford University, 450 Serra Mall, Stanford, CA 94305, USA

^c Department of Geological Sciences, Brown University, 324 Brook Street Box 1846, Providence, RI 02912, USA

^d Department of Earth and Environmental Sciences, Columbia University—Lamont-Doherty Earth Observatory, 61 Route 9 W Box 1000, Palisades, NY 10964, USA

ARTICLE INFO

Article history:

Received 21 December 2012

Received in revised form

8 April 2013

Accepted 21 May 2013

Editor: Y. Ricard

Available online 28 June 2013

Keywords:

Josephine Peridotite

shear zone

viscous anisotropy

mylonite

olivine

water

ABSTRACT

We present data from the Josephine Peridotite (SW Oregon, USA) that constrain the underlying physical processes responsible for the initiation of shear localization and the evolution of ductile shear zones in Earth's mantle. Field measurements of narrow (2–60 m wide) ductile shear zones in harzburgite were used to construct strain profiles, which have maximum shear strains ranging from $\gamma=5.25$ to $\gamma > 20$. Measurements of pyroxene water concentrations from harzburgite samples within and immediately adjacent to the shear zones indicate that gradients in water concentration exist on a 10–100 m scale, even after exhumation. Water concentration measurements are correlated with olivine lattice-preferred orientation (LPO), corroborating experimental results on the influence of water on slip system activity. Using empirical olivine flow laws and the diffusivity of water in olivine, we model initiation of a ductile shear zone through localized water weakening. We demonstrate that this mechanism can readily generate spatial perturbations in both effective viscosity and strain. However this model is not able to reproduce both the observed shear strain gradients and water concentration data from the Josephine shear zones. We evaluate other plausible localization mechanisms, which may amplify this initial strain perturbation. The most relevant at these conditions is the development of viscous anisotropy associated with the evolution of olivine LPO. Using recent experimental results, we demonstrate that progressive rotation of olivine LPO into the shear plane enhances deformation within a shear zone. We conclude that feedback between at least two microphysical processes is needed to account for observed outcrop-scale shear localization.

© 2013 Elsevier B.V. All rights reserved.

1. Introduction

Ductile shear zones are common features in the mantle sections of orogens and ophiolites (Drury et al., 1991; Ramsay, 1980). The importance of shear zones is well-established, as many authors have noted that localization is required for the initiation of subduction and the development of Earth-like plate tectonics (Bercovici, 2003; Bercovici and Ricard, 2012; Moresi and Solomatov, 1998; Regenauer-Lieb et al., 2001; Tackley, 1998; Trompert and Hansen, 1998). Moreover, shear zones may generate large-scale viscous anisotropy, which has been shown to influence patterns of lithospheric deformation (Lev and Hager, 2008; Tommasi et al., 2009). However many details of localization, including the sequence of and feedbacks between various microphysical processes are not well-constrained by geological observations.

To test hypotheses about shear localization at the outcrop scale, we collected field, compositional, and microstructural data for a suite of shear zones in the Josephine Peridotite (SW Oregon, USA). This peridotite massif represents the mantle section of a 150 Ma ophiolite that last equilibrated in a supra-subduction zone setting (Harding, 1988; Harper, 1984; Kelemen and Dick, 1995; Saleeby et al., 1982). The shear zones we discuss in this paper, and associated, localized melt transport conduits (dunites) are nearly vertical, and cut a sub-horizontal regional foliation. As with other ophiolites, we infer that the regional foliation was created by mantle upwelling and corner flow, in this case beneath a back-arc spreading center (Harper, 1984). Geothermometry indicates that the primitive, olivine-saturated melt that formed the dunites in our field area was stable in the Josephine mantle at ~ 1100 °C and 4–8 kb. In turn, the stability of primitive melt at such low temperatures requires that the melts were H₂O-rich, which is consistent with the interpretation of back-arc formation (Kelley et al., 2006), and is corroborated by the presence of hornblende in some genetically related, gabbroic dikes. Thus, the shear zones and

* Corresponding author. Tel.: +1 314 935 3584.

E-mail address: pskemer@wustl.edu (P. Skemer).

associated dunites formed off-axis, away from a spreading center, in the presence of hydrous melts, most likely above a subduction zone (Kelemen and Dick, 1995).

Shear zones in the Josephine were first identified by Loney and Himmelburg (1976), with subsequent descriptions by Harding (1988) and Kelemen and Dick (1995). Our focus has been on the Fresno Bench section of the Josephine Peridotite, a kilometer long outcrop consisting of harzburgite tectonite dissected by at least 10

sub-parallel, steeply dipping shear zones that vary in width from 2 to 60 m (Fig. 1) (Kelemen and Dick, 1995). The shear zones intersect a series of parallel, sub-horizontal pyroxenite layers. Passive rotation of these pyroxenite layers provides estimates of shear strain at every point across the shear zones (Skemer et al., 2010; Warren et al., 2008). Through comparison of strain measurements, water contents, and deformation microstructures, these shear zones provide a unique opportunity to study the

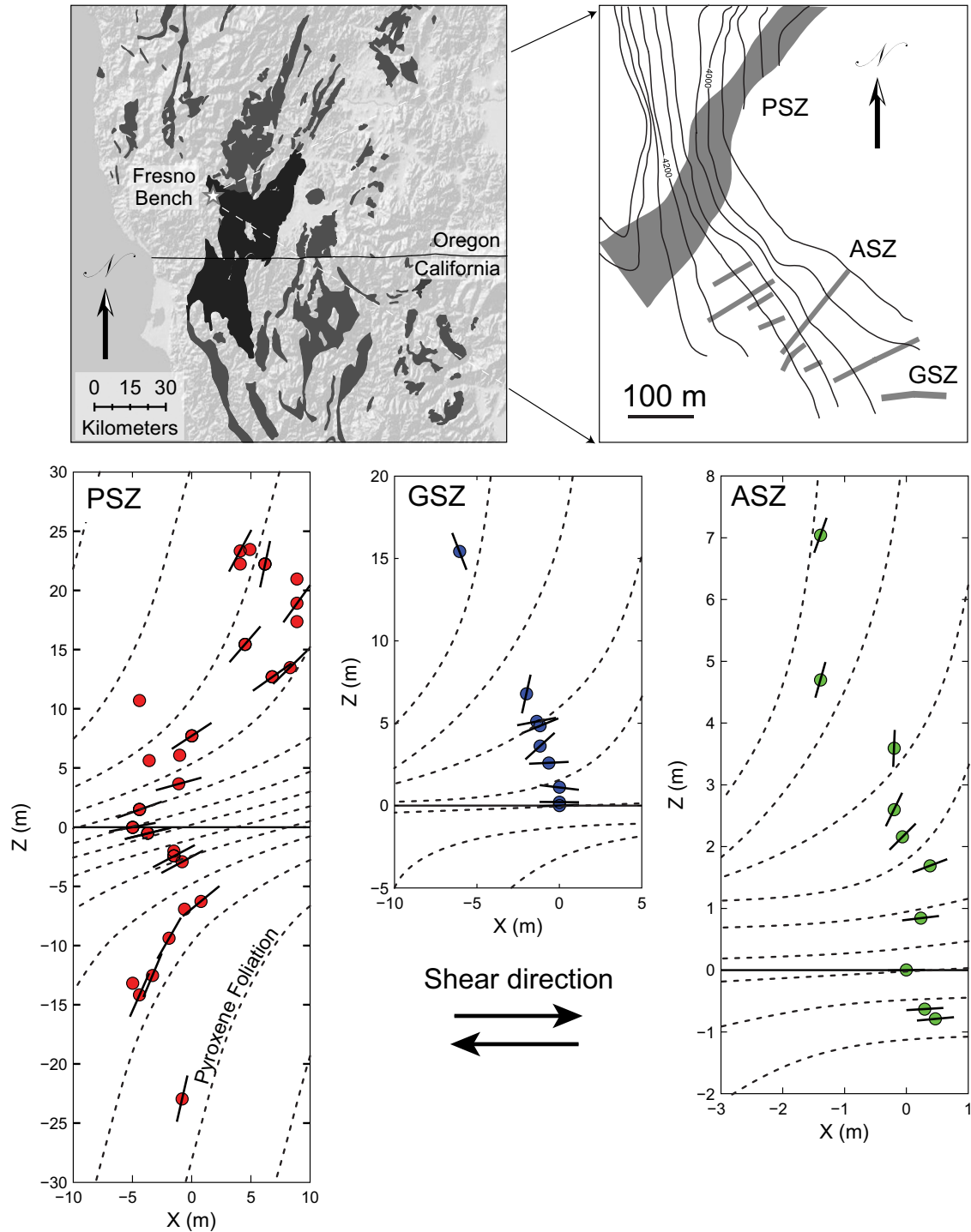


Fig. 1. Outcrop locations and transects of three shear zones through the Josephine Peridotite. Sample locations (circles) are projected into a plane perpendicular to the shear plane, where the X direction is parallel to the shear direction, and the Z direction is parallel to the shear-plane normal. Solid lines through the circles show the measured orientation of the associated pyroxene foliation, from which shear strain is calculated (see Warren et al. (2008), for a description of the methodology for calculating shear strain from pyroxene foliation). Dashed lines are schematic representations of the pyroxene foliation, to help with visualization of the strain field. The PSZ is the broadest and least localized shear zone in the study area, while GSZ and ASZ exhibit greater strain localization.

initiation and evolution of outcrop-scale localized deformation in Earth's mantle.

In this contribution, we present new data on water contents from several samples of the Fresno Bench outcrop. Water, in the form of hydrogen point defects in nominally anhydrous minerals, has a large influence on the rheological behavior of many silicate minerals e.g. (Kohlstedt, 2006). Local variations in water concentration provide one explanation for the initiation of strain localization. To investigate this effect, we model shear zone development in the presence of a localized water source. Because chemical diffusion will eventually relax any viscosity gradient arising from spatial variations in water concentration, the objective of the models is to determine the maximum perturbation in the strain-field that can be generated using reasonable geological and laboratory constraints. To better reproduce field and laboratory observations, we also consider the influence of changes in effective

viscosity (the viscosity of a non-linear material at a given flow stress) associated with the development of lattice-preferred orientation (LPO) (Hansen et al., 2012; Tommasi et al., 2009). Viscous anisotropy is parameterized using the recent experimental results of Hansen et al. (2012). We demonstrate that viscosity gradients caused by local perturbations in water content, amplified by the intrinsic viscous anisotropy of olivine, provide a plausible mechanism for shear zone initiation and evolution.

2. Description of Josephine shear zones

The shear zones through the Josephine Peridotite vary considerably in terms of width, shear strain, and petrologic evidence for melt–rock interaction. Microstructures within the shear zone range from porphyroclastic to proto-mylonitic to mylonitic. The deformation temperature of the shear zones, determined by two-pyroxene thermometry on dynamically recrystallized pyroxene neoblasts, is $\sim 1000^\circ\text{C}$ (Kelemen and Dick, 1995; Loney and Himmelburg, 1976; Skemer et al., 2010). For several of these shear zones, we have collected samples along transects perpendicular to the shear plane (Fig. 1). For each sample, shear strain is calculated from the rotation of adjacent pyroxenite layers (Fig. 2). Deformation microstructures of these samples were analyzed using optical and electron microscopy, and electron-backscatter diffraction (EBSD). See Warren et al. (2008) and Skemer et al. (2010) for further details of the strain measurements and microstructural analyses.

The study by Warren et al. (2008) investigated a broad shear zone (henceforth PSZ) with relatively modest strain ($\gamma_{\text{max}} \sim 5$). In PSZ, harzburgite is both interlayered with, and replaced by, dunite bands, which are interpreted to be a relict of channelized melt migration (Kelemen, 1990; Kelemen et al., 1995a; Quick, 1982). About 20 m from the sampling locality, a large 13 m wide dunite follows the strike of the shear zone. The formation of this large

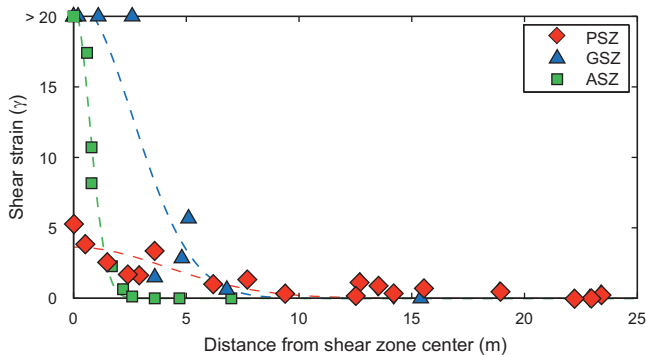


Fig. 2. Shear strain as a function of distance from the center of three Josephine shear zones described in this study. Points represent locations where pyroxene foliation was measured and samples were collected. Dashed lines are Gaussian fits to the data assuming shear zones are symmetric. Shear zone PSZ is the least localized, with a half-width of 10–15 m and a maximum shear strain of $\gamma \approx 5$.

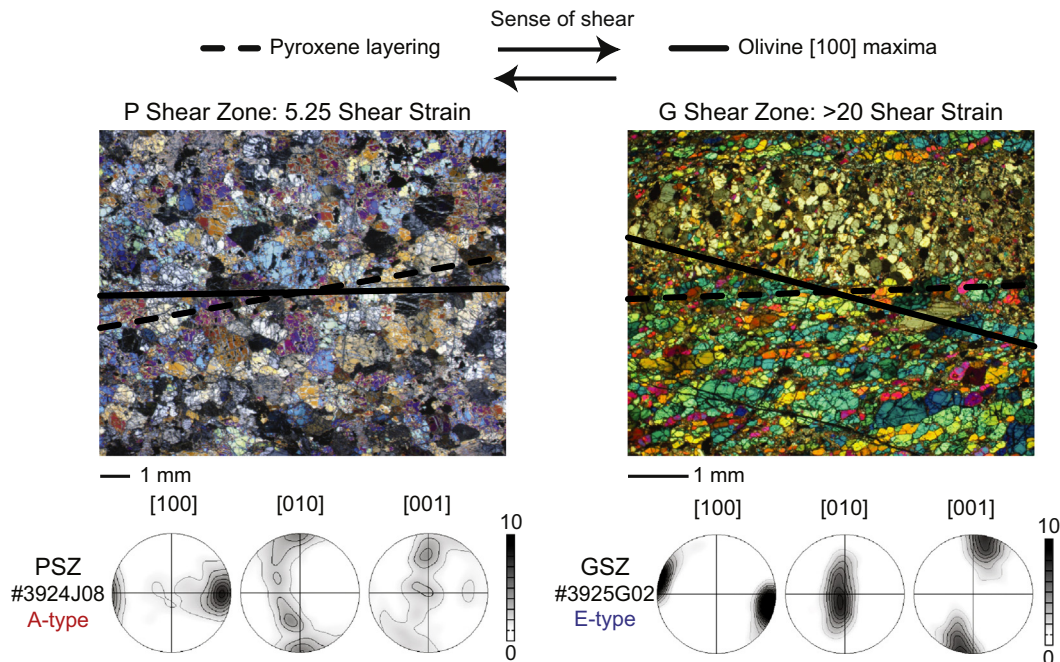


Fig. 3. Comparison of microstructures for the most deformed sample from PSZ and from GSZ. The highest strain sample from PSZ has the same average grain size (0.60 mm; Warren et al., 2008) as samples from outside the shear zone. In contrast, GSZ has undergone recrystallization to a grain size of 0.25 mm (Skemer et al., 2010). Solid lines represent field measurements of pyroxene foliation (indicating strain) and dashed lines show the orientation of the olivine [100] maxima determined by EBSD. Pole figures of A-type (Warren et al., 2008) and E-type (Skemer et al., 2010) LPOs for these samples are shown beneath. Lower hemisphere projections with the shear direction E–W and the pole to the shear plane N–S.

dunite is interpreted to have formed contemporaneously or after shear zone deformation (Kelemen and Dick, 1995; Morgan et al., 2008; Sundberg et al., 2010). Some of the smaller dunites, which appear to be deflected along with banding in the harzburgite, could pre-date PSZ, but some replace pyroxene-rich layers in the harzburgite (e.g., Fig. 3 in Kelemen and Dick, 1995) and could be syn- or post-kinematic.

Microstructural analyses of harzburgite samples by Warren et al. (2008) identified the development of an olivine A-type LPO (characterized by dominance of the [100](010) slip system), which are aligned with the shear plane at large strains (Fig. 3). Significantly, the authors did not observe any reduction in grain size across the shear zone. Average grain-sizes throughout the PSZ are ~0.5 mm. Skemer et al. (2010) investigated a second, more highly deformed shear zone (henceforth GSZ, $\gamma_{max} > 20$) that is not associated with any obvious magmatic features. A third shear zone, ASZ (Recanati et al., 2012), also reaches very large strains ($\gamma_{max} > 20$) and contains a 1–10 cm thick gabbro vein in its center. GSZ and ASZ both exhibit moderate grain-size reduction, including dynamic recrystallization of both olivine and orthopyroxene. In recrystallized domains, grain-size is reduced by approximately a factor of two. GSZ also shows development of a strong olivine E-type LPO (Fig. 3), which is characterized by the dominance of the [100](001) slip system and is interpreted to be a consequence of deformation under relatively water-rich conditions (Katayama et al., 2004; Mehl et al., 2003). In contrast to GSZ and ASZ, PSZ is broader and exhibits less strain, and will be used as the most conservative basis for comparison with our models.

3. Methods

3.1. Water concentration measurements

Hydrogen (water) concentrations in olivine, orthopyroxene and clinopyroxene were measured using the Cameca 6f Secondary Ion Mass Spectrometer (SIMS) at the Carnegie Institution of Washington. Measurements were made under ultra-high vacuum ($P < 10^{-9}$ Torr) using a rastered Cs^+ beam at a current of 15–20 nA. The rastered area was 30–40 μm , with ion collection limited to the central 10 μm diameter area through the use of a field aperture. Data were corrected for background water concentrations, which varied from 110 to 250 ppm H/Si (2σ error of 4–10%). Analytical reproducibility is estimated at 9%, based on repeat analyses of a homogeneous olivine grain. For minerals where only one point was analyzed, water concentration errors are based on error propagation that combines the analytical reproducibility (as this is larger than the count statistics error) and background water concentration error. For minerals with multiple data points, the standard deviation for the average of a set of analyses is reported; the standard deviation is larger than the error associated with individual data points. Calibration of the SIMS data was done using a set of mineral standards calibrated by a combination of FTIR, manometry and nuclear reaction (Koga et al., 2003). For standards calibrated by FTIR, concentrations are based on the Bell et al. (2003) FTIR calibration. The difference between the Bell et al. (2003) calibration and the earlier Paterson (1982) calibration is small for Opx, but significant for olivine (Koga et al., 2003). As discussed below, all conclusions in this study are derived from Opx water concentrations.

Late alteration was excluded as a possible cause for measured water concentrations by (i) checking for optical purity of the analyzed spot, (ii) monitoring C, S and Cl counts for any evidence of down-pit contamination, and (iii) multiple analyses per grain. Unlike FTIR, the SIMS technique does not provide information on the site occupancy of hydrogen in minerals. However, simple

Table 1

Flow law parameters for olivine under wet and dry conditions.

Parameter	Deformation mechanism	
	Wet dislocation creep	Dry dislocation creep
A^a	41.7	1.91E+05
n	3.5	3.5
R	1.2	0
E (kJ/mol)	480	530

^a Pre-exponential values are modified from Hirth and Kohlstedt (2003) to account for shear geometry (Paterson and Olgaard, 2000) and updated calibrations for water concentration measurements (Bell et al., 2003).

diffusion calculations demonstrate that hydrogen diffusion is too slow at temperatures relevant to serpentinization for alteration to have increased measured water concentrations. At 300 °C, the diffusion coefficient in olivine is 10^{-26} m²/s (Kohlstedt and Mackwell, 1999; Demouchy et al., 2006), which corresponds to an equilibration timescale of ~300 Gy for a grain of 1 mm radius. For further details of the method, see Hauri et al. (2002), Koga et al. (2003) and Warren and Hauri (in review).

3.2. Modeling shear localization in the presence of water concentration gradients

To test the influence of water concentration gradients on shear localization, we use a 1-D forward model that incorporates empirical olivine flow laws and hydrogen diffusion. Water is introduced as a 1 m wide zone of constant water concentration in the center of the model space. Water concentrations on either side of this source region are calculated using the analytical solution to the diffusion equation for semi-infinite half-spaces (Shewmon, 1989):

$$C_{OH}(x, t) = (C_i - C_b) \left[1 - \operatorname{erf} \left(\frac{x}{2\sqrt{Dt}} \right) \right] + C_b. \quad (1)$$

where C_{OH} is the concentration of water as a function of position and time, C_i is the concentration of water in the source region, C_b is the background water concentration far from the shear zone, x is the distance from the source region, and t is the time. We calculate volume diffusivity of hydrogen in olivine at 1000 °C to be $D_v = 10^{-11.8}$ m²/s based on Demouchy et al. (2006) and Kohlstedt and Mackwell (1999). For the purpose of the model we assume that negligible water is transported through grain boundaries. We justify this assumption by noting that the effective diffusivity is $D_{eff} = D_v + (\pi\delta/d)D_b$, where δ is the width of grain boundaries (~1 nm) (Hiraga et al., 2004), d is the grain size (~0.5 mm), and D_b is the grain boundary diffusivity. Measurements of grain boundary diffusivity by Demouchy (2010) demonstrate that at these conditions the contribution to bulk diffusion from flow along grain boundaries is much smaller than the contribution from volume diffusion. Differential stress and temperature are held constant throughout the model at 7 MPa and 1000 °C, respectively, which are values determined by grain-size piezometry and two-pyroxene thermometry for PSZ (Warren et al., 2008). The constant stress approximation is appropriate given force continuity constraints and the shear zone geometry.

Water concentration, stress, and temperature are incorporated into empirical flow laws for dislocation creep of olivine under both water-rich and water-poor conditions (Hirth and Kohlstedt, 2003).

$$\dot{\gamma}_{w,d} = F(\gamma) A \sigma^n C_{OH}^r \exp \left(-\frac{E^*}{RT} \right). \quad (2)$$

where $\dot{\gamma}_{w,d}$ is the shear-strain rate under either water-rich or water-poor conditions, σ is the differential stress, E^* is the

Table 2
Microstructural and water content data for samples described in this study.

Sample	Shear zone	Shear strain	Fabric type ^b	Water content (ppm H/Si) ^a			
				Olivine (measured)	Opx (measured)	Cpx (measured)	Olivine (calculated)
3923J01	PSZ	0	Relict	150 ± 50	1930 ± 170	–	270 ± 20
3924J08	PSZ	5.25	A-type	110 ± 10	2500 ± 220	–	350 ± 30
JP08PS01	GSZ	0	Relict	140 ± 30	3050 ± 440	5960 ± 520	430 ± 60
3925G01	GSZ	> 20	E-type	140 ± 10	3520 ± 300	–	490 ± 40

^a Olivine and pyroxene water concentrations were measured by SIMS using mineral standards from Koga et al. (2003). Calculated olivine water concentrations assume $D_{Opx/Ol} = 7 \pm 2$ based on water partitioning experiments from Aubaud et al. (2004), Hauri et al. (2006), and Tenner et al. (2009).

^b Relict fabrics are not related to the most recent deformation event.

activation energy, T is the temperature, and A , n , r , and R are constants (Table 1). F is a strain-dependent correction factor for modeling viscous anisotropy, as described below. The total strain-rate is assumed to be governed by the flow law that produces the fastest strain-rate at a given set of conditions. Strain-rates are evaluated by finite difference at each time step to calculate cumulative shear strain. Models are run until the maximum shear strain in the center of the shear zone is $\gamma=5$.

3.3. Modeling the effects of viscous anisotropy on shear localization

The influence of the pre-existing LPO on deformation is incorporated into the 1-D model using results from laboratory experiments reported by Hansen et al. (2012). Because the strength of the LPO does not vary significantly with increasing strain in the PSZ (Warren et al., 2008), we consider the maximum magnitude of viscous anisotropy to be constant throughout the model shear zone. Warren et al. (2008) measured a maximum LPO strength of $M=0.2$, where M is the M-index (Skemer et al., 2005). This value corresponds to a magnitude of viscous anisotropy of $\delta=6$, where δ is the ratio of the maximum and minimum viscosities (Hansen et al., 2012). The orientation of the LPO with respect to the shear plane varies systematically across the shear zone, and thus the effect of viscous anisotropy on the evolution of the shear zone will depend on the total accumulated strain. To account for this strain dependence, we assume the average olivine [100] direction relative to the shear direction, θ , is initially 45° and track rotation of the LPO as a function of strain. The function

$$\theta = \theta_i \exp\left(\frac{-\gamma^2}{5.12}\right). \quad (3)$$

where θ_i is the initial orientation and γ is the shear strain, approximates the fabric orientations observed in the PSZ by Warren et al. (2008). This function is also broadly consistent with other geological and experimental observations, reinforcing the general applicability of experimental data on LPO evolution (Skemer et al., 2012). At each time step the fabric orientation is used to calculate an adjustment factor, F , for the strain rate provided by empirical olivine flow laws, which is determined by

$$F = (F_n - F_s) \sin(2\theta) + F_s \quad (4)$$

The parameters F_n and F_s refer to the correction factors for pure-shear deformation in the strongest orientation and simple-shear deformation in the weakest orientation, respectively. Values of $F_n=0.5$ and $F_s=2.8$ are calculated from the results of Hansen et al. (2012) for $\delta=6$. This phenomenological model only considers the orientation of [100] maxima and therefore does not account for differences in viscosity between A- and E-type fabrics. However, we assert that these two fabrics should result in similar anisotropy in viscosity because experiments on olivine single crystals reveal that (010)[100] and (001)[100] slip systems have similar effective viscosities under a wide range of conditions, e.g.

(Bai et al., 1991; Mackwell et al., 1985), although the presence of water results in a modest enhancement of (001)[100] relative to (010)[100].

4. Results

4.1. Water concentrations in shear zones

Water concentrations vary from 110 to 150 ppm H/Si in olivine and from 1930 to 3520 ppm H/Si in orthopyroxene (Table 2). Clinopyroxene from sample JP08PS01 has 5960 ppm H/Si, while clinopyroxene grains in all other samples were too small for recovery and analysis. Results for each sample are the average of 1–6 points analyzed in 1–3 grains per sample. Errors in Table 2 represent 2σ standard deviation on these averages.

Several lines of reasoning suggest that olivine has diffusively lost water during cooling and emplacement, while pyroxenes retain their high temperature compositions. Comparison of individual analyses of cores and rims of olivine grains shows higher concentrations in some cores compared to rims. For example, the rim (140 ppm H/Si) of an olivine grain from sample 3923J01 has a significantly lower water concentration than its core (230 ppm H/Si). In contrast, pyroxene core and rim concentrations are the same in all samples, within analytical error (Warren and Hauri, in review). The higher concentrations of water in the olivine cores also demonstrate that water has been lost from the system, not added during a late stage hydration event.

Another line of evidence that indicates water loss from olivine, but not orthopyroxene or clinopyroxene, comes from the calculation of mineral/mineral partition coefficients. Using our H/Si data, the partition coefficient for hydrogen between orthopyroxene and olivine ($D_{Opx/Ol}$) ranges from 13 to 26. These values are significantly greater than the value determined experimentally, $D_{Opx/Ol} = 7 \pm 2$, which is the average of 11 experiments from Aubaud et al. (2004), Hauri et al. (2006), and Tenner et al. (2009)). A value of $D_{Cpx/Ol} = 41$ was measured for sample JP08PS01, which is also high compared to the experimentally determined value of $D_{Cpx/Ol} = 12 \pm 4$ (eight experiments). In both cases, the high partition coefficients for the Josephine samples are best explained by water loss from olivine.

In contrast to olivine, the partitioning of water between clinopyroxene and orthopyroxene in the Josephine samples gives $D_{Cpx/Opx} = 2.0$. This value is close to the experimentally determined value of $D_{Cpx/Opx} = 1.4 \pm 0.3$ (10 experiments) and overlaps the literature range for xenoliths of $D_{Cpx/Opx} = 2.6 \pm 0.9$ (141 samples). The apparent equilibrium partitioning between clinopyroxene and orthopyroxene in the Josephine samples suggests that both of these minerals have retained their original water contents. Our interpretation that olivine, but not pyroxene, has undergone water loss is in agreement with previous studies of peridotite xenoliths (Demouchy et al., 2006; Peslier and Luhr, 2006), which did not find evidence for significant water loss from pyroxenes. Despite the

slower exhumation rate, the potential for water loss from large (1–100 km) peridotite massifs, which are presumably surrounded by water saturated rock, should be lower than for xenoliths, which are generally < 10 cm in diameter and surrounded by magma with low water activity.

For the two shear zones analyzed (PSZ and GSZ), orthopyroxene water contents are higher in the shear-zone centers than at the margins (Table 2). In the center of the PSZ, orthopyroxene contains 2500 ppm H/Si. In the low strain margin of this shear zone, orthopyroxene contains 1930 ppm H/Si. Likewise, in GSZ, the orthopyroxene water content varies from 3520 ppm H/Si at the center of the shear zone to 3050 ppm H/Si along the shear zone margin (Fig. 4a).

Olivine water concentrations during deformation can be calculated from orthopyroxene water concentrations. Using the experimentally

determined value of $D_{Opx/Ol} = 7$ (Aubaud et al., 2004; Hauri et al., 2006; Tenner et al., 2009) this calculation yields olivine concentrations of 270–350 ppm H/Si in PSZ and 430–490 ppm H/Si in GSZ (Table 2). The dataset for $D_{Opx/Ol}$ corresponds to a total of 12 experiments, which show no systematic variation as a function of mineral composition or pressure. Warren and Hauri (in review) discuss the experimental dataset in detail and its relevance to natural samples. The absolute amount of calculated water in olivine may change when more data becomes available for $D_{Opx/Ol}$. However, the relative variation among the Josephine samples is based on pyroxene water concentrations and will not change. For PSZ, the calculated olivine water concentrations demonstrate differences among the samples that are significantly larger than the analytical error of the measurements (Table 2; Fig. 4a). At these deformation conditions, the water concentrations in olivine of several hundred ppm H/Si have a large effect on rheology (Hirth and Kohlstedt, 2003).

In addition to the influence of water on rheology, the presence of water can modify the olivine LPO pattern through its influence on the relative activity of olivine's principal slip systems (Jung and Karato, 2001). In the Josephine shear zones, two different types of LPOs have been identified at high strain: olivine A-type in PSZ, characterized by dominance of the $[100](010)$ slip system and olivine E-type in GSZ, characterized by dominance of the $[100](001)$ slip system (Fig. 4b). The transition between these two LPO types has been determined experimentally to depend mainly on water content (Fig. 4b), although the precise location of the boundary is not well resolved by the data (Jung et al., 2006; Karato et al., 2008). The observation of the olivine E-type LPO in the high strain GSZ sample is consistent with the higher olivine water content (490 ppm H/Si in olivine) calculated for the GSZ based on the SIMS measurements. In contrast, the PSZ exhibits an olivine A-type LPO, consistent with its lower calculated olivine water content (350 ppm H/Si).

The transition from A-type to E-type LPOs in the Josephine shear zones occurs at a similar water content to the transition inferred from extrapolation of laboratory data to lower differential stresses, supporting the interpretation that the transition is dependent mainly on water content (Fig. 4b). The Josephine samples actually provide a refinement of the location of the transition from A-type to E-type LPOs, suggesting that it occurs between 350 and 490 ppm H/Si. The consistency between the water contents calculated from SIMS measurements and the water contents expected from olivine LPOs provides further evidence that gradients in water concentration existed over relatively small length scales during the localized deformation.

4.2. Model results

In our models of shear localization we evaluate a range of initial water concentrations, varying both the source (C_i) and the background (C_b) concentrations from 0 to 1000 ppm H/Si in olivine. For most models, the source and background concentrations are held constant throughout the duration of deformation. The absence of an E-type LPO in PSZ provides an upper limit to the water concentration that could have been present during deformation of this particular shear zone (~500 ppm H/Si). An additional constraint is provided by the experimentally determined solubility of water in olivine at these conditions: at $T = 1273$ K and $P = 0.5$ GPa, the maximum solubility of water in olivine is 690 ppm H/Si (Zhao et al., 2004). The results of two models are shown in Fig. 5. The first model has a background water concentration of 270 ppm H/Si (Fig. 5a–c), which is the water concentration of the undeformed sample from outside PSZ (sample 3923J01, Table 2). The second model has a background water concentration of 0 ppm H/Si (Fig. 5d–f). Both models have 350 ppm H/Si in the center of the shear zone, which is the olivine water concentration estimated

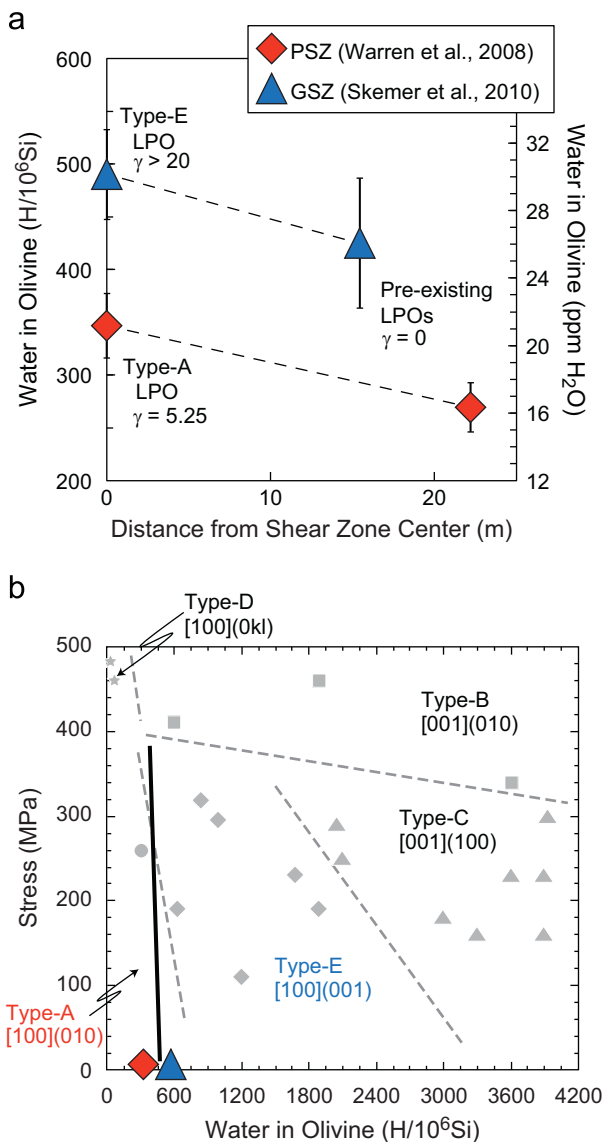


Fig. 4. (a) Calculated water concentration in olivine based on measured orthopyroxene water concentrations, plotted as a function of distance from the center of PSZ and GSZ. Olivine fabric types as noted. (b) Variation in olivine LPO as a function of stress and water content, modified from Jung et al. (2006). Gray points are previously published data from laboratory experiments. Water contents for the experiments are adjusted by a factor of three to agree with the calibration of Bell et al. (2003). The dashed lines are the location of the experimentally inferred fabric transitions from Katayama et al. (2004). While the location of the A-type to E-type transition is not well-constrained, particularly at low stress, experimental results are in good agreement with the geological observations (solid line).

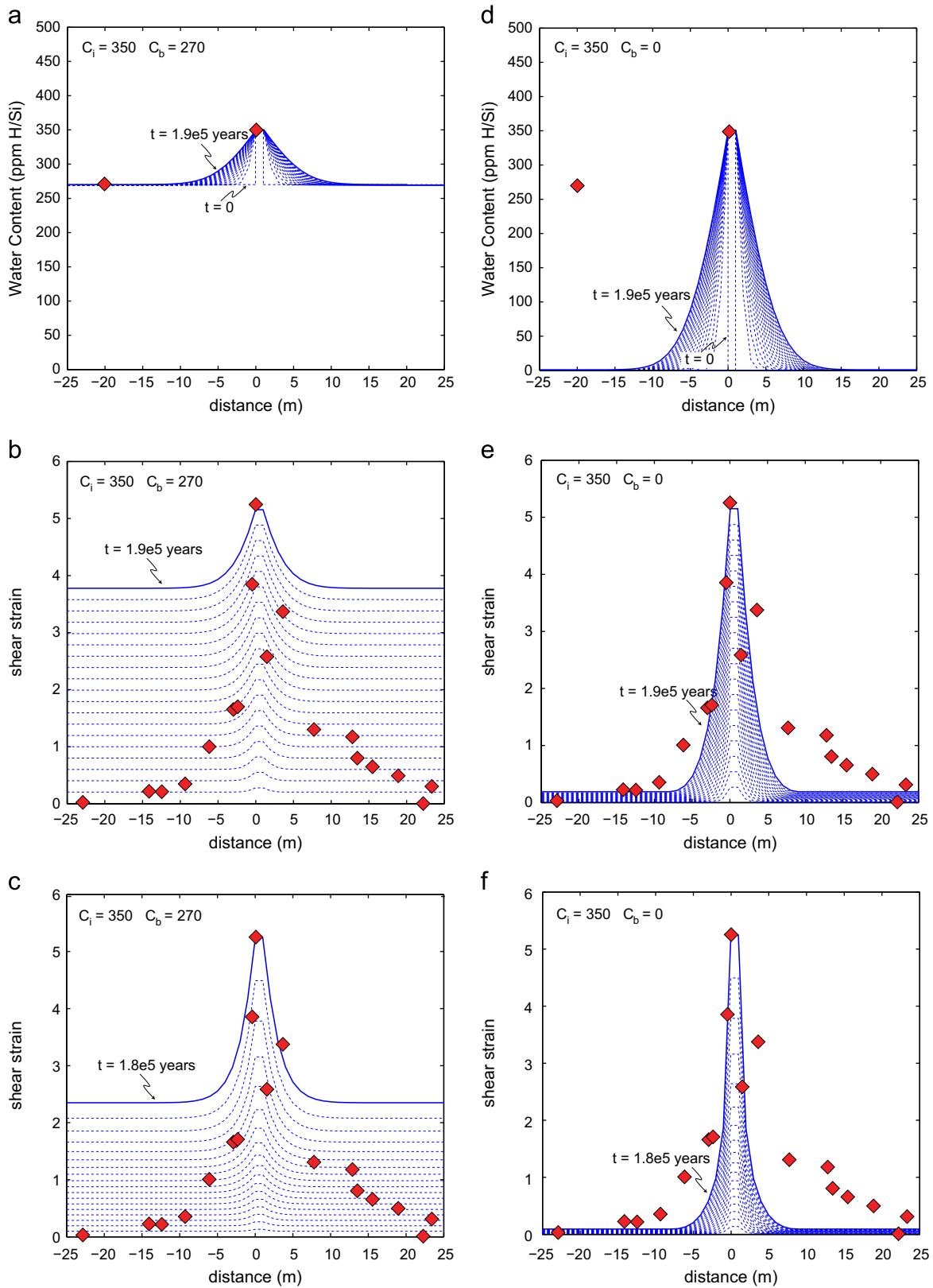


Fig. 5. Water content evolution and strain development in a model shear zone, with data from PSZ (red diamonds) superimposed on the models. All models are run until the maximum shear strain in the center of the model is $\gamma=5$ (solid lines). Each contour corresponds to a time-step of 10^4 yr. (a, d) Water concentration profiles, which broaden with time. (b, e) Strain profile assuming only water weakening (no viscous anisotropy from LPO). (c, f) Strain profile including the effects of both water weakening and LPO development. Left: model with initial water concentrations of $C_i=350$ ppm H/Si and $C_b=270$ ppm H/Si. This model reproduces observed water concentrations, but generates too much strain in the far field to be consistent with observations. Right: model with initial water concentrations of $C_i=350$ ppm H/Si and $C_b=0$ ppm H/Si. This model does a reasonable job of matching the observed strain profile of PSZ, but the background water concentration is much lower than measured. (For interpretation of the references to color in this figure legend, the reader is referred to the web version of this article.)

for sample 3924J08 (Table 2). The amplitude and width of the shear zone depend on the viscosity gradient imposed by the water concentration perturbation and the diffusivity of the water. Small diffusivities and large perturbations in water concentration enhance localization. Models with lower overall water concentrations accumulate strain more slowly, which allows the width of the shear zone to increase.

While all models produce some degree of strain localization, we are not able to simultaneously reproduce both the strain profile and the water concentration profile from PSZ through the rheological effects of water alone. Models that reproduce the strain profile have very low water concentrations in the far-field, which is inconsistent with measurements (Fig. 5d and e). Models that reproduce the observed gradient in water content generate too much strain in the far-field to be consistent with the field observations (Fig. 5a and b).

We evaluate the role of viscous anisotropy by modifying the standard constitutive expression for strain-rate by a factor F (Eqs. (2)–(4)), to account for the strength and orientation of the crystallographic fabric (Fig. 5c and f). Assuming a simple shear geometry, the initial orientation of the [010] axis maxima is approximately parallel to the maximum compressive stress (Warren et al., 2008). Based on laboratory experiments on olivine aggregates with a strong LPO (Hansen et al., 2012), this fabric orientation relative to the principal stresses exhibits the highest viscosity. Therefore, all points in our anisotropic model begin with an effective viscosity higher than that of an isotropic aggregate; the effective viscosity in the shear zone then decreases with increasing strain. Viscous anisotropy preferentially reduces effective viscosity where modest strain has already accumulated. Thus, the viscosity contrast caused by the higher water concentration in the center of the shear zone is amplified due to the evolving olivine fabric. This scenario results in an increase in the degree of localization. As illustrated through comparison of Fig. 5b, e and c, f, viscous anisotropy increases the ratio between the maximum shear zone strain and the background strain by a factor of ~ 2 .

5. Discussion

The shear zones in the Josephine Peridotite provide an opportunity to study the relationships between strain, rheology, water content, and microstructure, providing a framework for evaluating the initiation of localization in mantle shear zones. Potential underlying processes for shear localization have been reviewed in a number of places e.g., (Bercovici and Karato, 2002; Drury et al., 1991; Kelemen and Hirth, 2007; Montesi and Zuber, 2002; Regenauer-Lieb and Yuen, 2003). We discuss the five mechanisms (water content, viscous anisotropy, grain size, shear heating, and melt content) that are most relevant in the context of high temperature deformation, and consider their role in the initiation and subsequent evolution of the Josephine Peridotite shear zones.

5.1. The role of water

The premise of our study is that local variations in water concentration may have helped initiate shear localization within the Josephine Peridotite. The measurements of hydrogen in orthopyroxene indicate that gradients in water concentration exist from the centers to the margins of the shear zones, even after exhumation. E-type LPOs observed in GSZ (Skemer et al., 2010) suggest that elevated water concentrations (> 500 ppm H/Si) were present in some rocks during deformation (Jung et al., 2006), while the presence of an A-type LPO throughout the PSZ indicates that the water content in this particular shear zone was

somewhat lower (Fig. 4). Hence, we conclude that gradients in water content existed at multiple length scales (10–100 m) during the period of high temperature deformation. Outcrop-scale variation in olivine fabrics have also been observed recently within the Oman Ophiolite, just beneath the Moho (Michibayashi, pers. com. 2011).

The results of our models indicate that gradients in water concentration can produce perturbations in the strain-field of a shear zone (Fig. 5). However, diffusion of water out of the shear zone acts as a negative feedback, decreasing the tendency for localization. Hence, a shear zone generated by water weakening broadens with time. Our models are constructed to produce the maximum localization effect. For example, if models are supplied with a finite water supply, or if lateral transport of water is more rapid (e.g. through porous flow or via enhanced diffusion), the tendency for localization would be reduced. None of our models reproduced both the strain-profile and the water concentration gradient from PSZ through water weakening alone. However, we do find that large perturbations in strain ($d\gamma > 1$) can be generated over length scales consistent with the dimensions of the Josephine shear zones. As discussed below, these perturbations in strain may be amplified by other microphysical feedback mechanisms (particularly viscous anisotropy), generating larger strains within narrower shear zones.

5.2. The role of LPO

Strain localization may be enhanced by the development of LPO, which forms due to the intrinsic viscous anisotropy of crystalline materials. In general, certain slip systems accommodate deformation more easily than others, causing preferential rotations of crystal lattices during dislocation creep e.g. (Wenk, 1985). When a rock exhibits a strong LPO, the average mechanical properties begin to approach those of a single crystal. There is a limit to the magnitude of weakening that can be achieved, which is related to the relative strengths of the slip systems, and the saturation of LPO strength. In recent experiments by Hansen et al. (2012), the authors observe progressive strain weakening in olivine aggregates. At modest strains ($\gamma < 3$), the experimental observations demonstrate a reduction in viscosity related to LPO development, corroborating the numerical calculations of Tommasi et al. (2009). At large strains ($\gamma > 10$), Hansen et al. observe that the strength in the weakest orientation during constant strain rate experiments is approximately 40% less than the strength in the strongest orientation. This corresponds to roughly an order of magnitude reduction in effective viscosity under constant stress conditions, depending on the stress exponent in the power-law relationship between stress and strain-rate. While the influence of LPO on viscosity is an appealing explanation for localization, field observations and laboratory experiments indicate that a substantial initial perturbation in strain ($d\gamma > 1.5$) is required to generate a gradient in LPO orientation and strength (Skemer et al., 2012; Warren et al., 2008). Hence, strain localization due to LPO formation alone cannot arise spontaneously, but must develop in combination with another localization mechanism. We suggest that the presence of a spatially variable water concentration provides an initial perturbation for shear zone formation, initiating the re-alignment of LPO within the shear plane and giving rise to long term weakening due to viscous anisotropy. Our models demonstrate that the inclusion of viscous anisotropy increases the contrast in shear strain from the center to the margin of the shear zone by at least a factor of two.

5.3. The role of grain size

Grain-size reduction is often observed in association with localized deformation and is thought to play a role in the

weakening of mylonites and ultramylonites in a variety of mantle and crustal settings (Jaroslow et al., 1996; Jin et al., 1998; Montes and Hirth, 2003; Vissers et al., 1997; Warren and Hirth, 2006; White et al., 1980). To promote strain localization, the reduction in grain-size must induce a transition from the dislocation creep deformation regime to a grain-size sensitive regime e.g. (Rutter and Brodie, 1988). Sufficient strain is also required to fully recrystallize the rock, which requires a substantial perturbation to the strain-field. Across GSZ, there is a reduction in the olivine grain-size from $\sim 550 \mu\text{m}$ to $\sim 250 \mu\text{m}$ (Fig. 3). However, at the inferred conditions for deformation this reduction is not sufficient to induce a change in the olivine deformation mechanism from dislocation creep to grain-size sensitive creep (Skemer et al., 2010). Across PSZ, there is no resolvable variation in grain-size (Warren et al., 2008). Therefore, we conclude that grain-size reduction does not contribute to localization in this particular setting. The absence of grain-size variation across PSZ also suggests that the assumption of constant stress is valid, as gradients in stress should produce gradients in recrystallized grain-size e.g. (Twiss, 1977).

5.4. The role of shear heating

Shear heating is another important feedback mechanism, linking heat produced by mechanical dissipation to the strong temperature dependence of plastic deformation (Fleitout and Froidevaux, 1980; Kelemen and Hirth, 2007; Schubert and Yuen, 1978; Yuen et al., 1978). In the Josephine Peridotite, estimated stresses (5–20 MPa) (Skemer et al., 2010; Warren et al., 2008) and plausible strain-rates (10^{-12} – 10^{-13} s^{-1} for these stresses, based on grain size piezometry, geothermometry, and olivine flow laws) are relatively low and the heat produced by deformation is likely small. Moreover, the background temperature for deformation in these shear zones ($\sim 1000 \text{ }^\circ\text{C}$) is higher than many peridotite mylonites ($\sim 700 \text{ }^\circ\text{C}$) (Jaroslow et al., 1996; Linckens et al., 2011). As shown by Kelemen and Hirth (2007), shear heating instabilities for olivine rheologies do not develop at ambient temperatures above about $800 \text{ }^\circ\text{C}$. Hence, at these deformation conditions, shear heating is not expected to enhance localization.

5.5. The role of melt

Melt has a significant effect on peridotite rheology (Hirth and Kohlstedt, 1995). The segregation of melt into high permeability/low viscosity channels has been proposed as a feedback mechanism for localizing deformation (Stevenson, 1989). Recent work in the Oman Ophiolite has indicated that melt may contribute to weakening in the end-member case where large melt fractions are present at the crust–mantle transition zone (Higgie and Tommasi, 2012). As such, it is important to consider how melt may have contributed to localized deformation in the Josephine Peridotite. The Josephine Peridotite as a whole is interpreted to represent the product of pervasive partial melting, which resulted in the formation of harzburgite (Dick, 1976, 1977; Kelemen et al., 1997). The harzburgite is overprinted by a series of later stage magmatic events, including channelized zones of partial melt. The primary evidence for channelized melt migration is the presence of replacive dunites, which are left behind by the preferential dissolution of pyroxene (Braun and Kelemen, 2002; Kelemen et al., 1995a, 1995b; Quick, 1982). In the Josephine, there are spatial and temporal correlations between shear zones and replacive dunites, which led Kelemen and Dick (1995) to conclude that melt migration and shear localization were coeval.

However, not all of the shear zones contain evidence for localized melt transport. Other shear zones that contain significant evidence for channelized melt (i.e. relict dunites) are still predominantly composed of sheared harzburgite. For example, GSZ

contains pyroxenite veins, but these appear to have crystallized prior to deformation. A large dunite follows the PSZ, but the lack of macroscopic deformation features in the dunite suggests that it last recrystallized after deformation ended in PSZ. While the Josephine harzburgites reacted with melt migrating by focused flow in porous conduits (Morgan et al., 2008), it is unclear whether melt accumulated in sufficient volumes to influence deformation. Takei and Holtzman (2009) demonstrated that large reductions in viscosity can occur at low melt-fractions in the diffusion creep regime. Experimental data on dunites and lherzolites indicate that melt contents in the range of 5–10% are required to decrease effective viscosity by an order of magnitude in the dislocation creep regime (Hirth and Kohlstedt, 1995; Zimmerman and Kohlstedt, 2004). However, studies employing a combination of model results and field observations have inferred a maximum melt fraction of about 3% in active dissolution channels that are thought to form dunite conduits (Braun and Kelemen, 2002; Spiegelman and Kelemen, 2003; Spiegelman et al., 2001). Larger strains may have been accommodated in the replacive dunites; however this possibility is impossible to quantify because strain markers (i.e. pyroxene bands) were destroyed by the dunite formation process.

Based on these rheological and petrological considerations, we conclude that partial melt was not the primary cause of shear localization, although it may have played a secondary role. Indeed, the presence of melt likely provided the initial water perturbation that led to localized weakening. Thus, the most important effect of melt in the Josephine shear zones may have been as the source of the elevated water contents rather than through its direct influence on rheology.

5.6. Additional factors

Our model (Fig. 5) demonstrates that a combination of water weakening and LPO development can generate narrow shear zones in a manner consistent with known experimental data. However we are not able to simultaneously reproduce both the strain-profile and water concentration profile of PSZ. There are a number of additional factors that could explain the discrepancy between our models and our geologic observations.

First, we only have information about water concentrations after exhumation. We do not know if water contents changed during the deformation event. One plausible scenario is that water concentrations in the center of the shear zone started out closer to the solubility limit and decreased over time, due to finite supply and diffusion into the country rock. The observation of the A-type fabric in PSZ suggests that the final strain increment ($d\gamma \sim 1$) accumulated in an environment with less than $\sim 500 \text{ ppm H/Si}$. However we cannot rule out the possibility that an earlier part of the strain history took place when a larger water concentration gradient was present. In Fig. 6 we show a model where the water content was reduced when shear strain reached $\gamma=4$, simulating water loss from the shear zone center due to diffusion or a decrease in the source concentration. While admittedly speculative, such models can qualitatively reproduce both the water concentration and strain profiles of the PSZ.

Second, there is uncertainty in the amount of partial melt that could be present within the deforming harzburgite. While we have ruled out the hypothesis that all localization resulted from gradients in melt content, we cannot discount the possibility that a small amount of melt was present in parts of the shear zone during deformation. The presence of $\sim 2\%$ partial melt for some period during deformation could locally reduce the effective viscosity by a factor of two in the dislocation creep regime (Hirth and Kohlstedt, 1995), without significantly modifying the relative modal abundances of olivine and orthopyroxene.

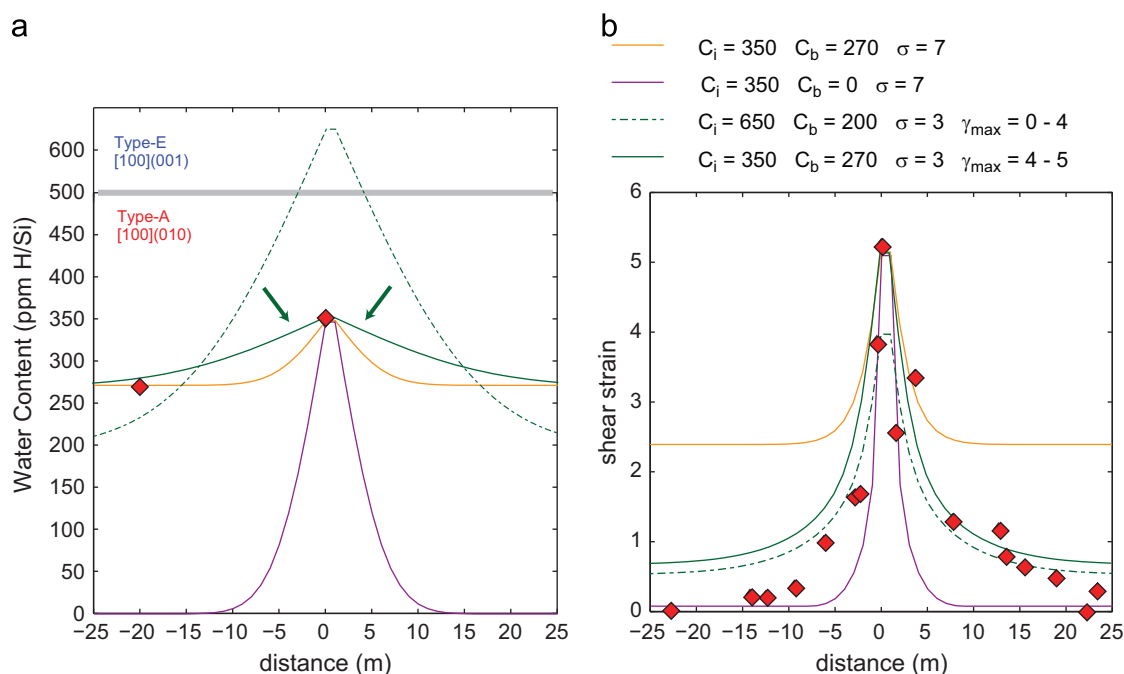


Fig. 6. Exploration of parameter space for models that include the effects of both water and viscous anisotropy. The orange and purple curves are identical to the final time steps from Fig. 5c and f. The green curves illustrate one plausible explanation for the observed shear strain and water concentration profiles. Two details in the model are modified. (1) The shear stress is reduced to 3 MPa, decreasing the strain-rate and causing the shear zone to broaden. (2) Water concentrations are reduced when the maximum shear strain in the model reaches $\gamma=4$ (green dashed line), so the peak water concentration at the final time step is within the A-type regime (green solid line). This modification allows us to reproduce both final water concentration and strain-profiles, as well as the observed olivine LPO. (For interpretation of the references to color in this figure legend, the reader is referred to the web version of this article.)

Third, additional uncertainties arise from the extrapolation of flow laws, and the experimentally calibrated relationship between recrystallized grain-size and stress. For example, it is reasonable to hypothesize that actual flow stresses varied by a factor of two from the value imposed in the model (7 MPa). Moreover, experimental error in the value of the stress exponent for dislocation creep results in an uncertainty of approximately an order of magnitude in strain rate after extrapolation to mantle conditions. Variations in strain rate change the time scale of deformation across the entire shear zone, which can result in a wider or narrower shear zone (Fig. 5).

Fourth, there is also uncertainty in the ratio of shear zone strain to the far field strain (and thus in the ratio of effective viscosity across the shear zone) because the initial orientation of the pyroxene bands is not precisely known. In our analysis we made the assumption that the far-field strain is essentially zero (Fig. 2). However, small strains could have been accommodated in the far-field (i.e. pyroxene bands may have originally been oriented at a higher angle to the shear zone). Because there is generally no evidence for shortening/folding of the pyroxene bands outside of the shear zone, we conservatively estimate that the initial pyroxene band orientation was at most 110° from the shear zone. In this case, all strain measurements could be increased by up to $\gamma=0.5$ (Warren et al., 2008). Such a scenario significantly reduces the ratio of the shear zone strain to the far-field strain (i.e., $5/0.1=50$, while $5.5/0.6=9.2$), providing a closer fit between the model and the observed strain gradient.

6. Conclusions

In the Josephine Peridotite, deformation in ductile shear zones is a manifestation of localized rheological weakening. Although many microphysical mechanisms for shear localization have been

proposed, no single mechanism can explain the shear zone initiation, the magnitude of weakening, and the narrowness of the zone of deformation. Therefore, we conclude that some combination of effects must be responsible.

Gradients in water content from the centers to the margins of the shear zones suggest that an initial perturbation in viscosity may have been caused by localized water weakening. This perturbation, potentially enhanced by a small fraction of melt, initially concentrated strain into the water-rich domain, leading to the development of a strong LPO aligned with the shear plane. Further localization is generated by the contrast in viscosity between strongly aligned olivine within the shear zone and relatively weakly aligned olivine outside of the shear zone. The perturbations in water content are interpreted to originate from the localized flow of hydrous melts, which also generated the relict dunite channels.

Continued evolution of these shear zones may introduce other effects, such as grain-size sensitive deformation or shear heating. Grain-size reduction, in particular, may be critical for the long-lived mechanical weakness of shear zones at lower temperatures. However, field and microstructural observations indicate that these mechanisms did not play a significant role in the initial formation of the Josephine mantle shear zones.

Acknowledgments

The authors wish to thank Erik Hauri for his assistance with hydrogen measurements. Yanick Ricard (AE) and two anonymous reviewers are thanked for their constructive input. This project was supported by the NSF EAR-0911289 (to Skemer), EAR-0948609 and EAR-1255620 (to Warren), EAR-0738880 (to Hirth), and EAR-0739010 (to Kelemen).

References

- Aubaud, C., Hauri, E.H., Hirschmann, M.M., 2004. Hydrogen partition coefficients between nominally anhydrous minerals and basaltic melts. *Geophys. Res. Lett.* 31, L20611.
- Bai, Q., Mackwell, S.J., Kohlstedt, D.L., 1991. High-temperature creep of olivine single crystals 1. Mechanical results for buffered samples. *J. Geophys. Res.* 96, 2441–2463.
- Bell, D.R., Rossman, G.R., Maldener, J., Endisch, D., Rauch, F., 2003. Hydroxide in olivine; a quantitative determination of the absolute amount and calibration of the IR spectrum. *J. Geophys. Res.-Solid Earth* 108, 2105.
- Bercovici, D., 2003. The generation of plate tectonics from mantle convection. *Earth Planet. Sci. Lett.* 205, 107–121.
- Bercovici, D., Karato, S.-i., 2002. Theoretical analysis of shear localization in the lithosphere. In: Karato, S.-i., Wenk, H.R. (Eds.), *Plastic Deformation of Minerals and Rocks*. Mineralogical Society of America and Geochemical Society, Washington, DC, United States.
- Bercovici, D., Ricard, Y., 2012. Mechanisms for the generation of plate tectonics by two-phase grain-damage and pinning. *Phys. Earth Planet. Inter.* 202–203, 27–55.
- Braun, M.G., Kelemen, P.B., 2002. Dunite distribution in the Oman ophiolite: implications for melt flux through porous dunite conduits. *Geochem. Geophys. Geosyst.* 3, 8603.
- Demouchy, S., Jacobsen, S.D., Gaillard, F., Stern, C.R., 2006. Rapid magma ascent recorded by water diffusion profiles in mantle olivine. *Geology* 34, 429–432.
- Demouchy, S., 2010. Diffusion of hydrogen in olivine grain boundaries and implications for the survival of water-rich zones in the Earth's mantle. *Earth and Planet. Sci. Lett.* 295, 305–313.
- Dick, H.J.B., 1976. The Origin and Emplacement of the Josephine Peridotite of Southwestern Oregon. Yale University, New Haven CT, p. 409.
- Dick, H.J.B., 1977. Partial melting in the Josephine Peridotite 1. Effect on mineral composition and its consequence for geobarometry and geothermometry 277, 801–832. *Am. J. Sci.* 277, 801–832.
- Drury, M.R., Vissers, R.L.M., Van, d.W.D., Hoogerduijn, S.E.H., 1991. Shear localisation in upper mantle peridotites. *Pure Appl. Geophys.* 137, 439–460.
- Fleitout, L., Froidevaux, C., 1980. Thermal and mechanical evolution of shear zones. *J. Struct. Geol.* 2, 159–164.
- Hansen, L.N., Zimmerman, M.E., Kohlstedt, D.L., 2012. Laboratory measurements of the anisotropic viscosity of olivine. *Nature* 492, 415–418.
- Harding, D., 1988. Josephine Peridotite Tectonics: A Record of Upper-Mantle Plastic Flow. Cornell University, Ithaca NY, p. 334.
- Harper, G.D., 1984. The Josephine Ophiolite, Northwestern California. *Geol. Soc. Am. Bull.* 95, 1009–1026.
- Hauri, E., Wang, J.H., Dixon, J.E., King, P.L., Mandeville, C., Newman, S., 2002. SIMS analysis of volatiles in silicate glasses 1. Calibration, matrix effects and comparisons with FTIR. *Chem. Geol.* 183, 99–114.
- Hauri, E.H., Gaetani, G.A., Green, T.H., 2006. Partitioning of water during melting of the Earth's upper mantle at H₂O-undersaturated conditions. *Earth Planet. Sci. Lett.* 248, 715–734.
- Higgie, K., Tommasi, A., 2012. Feedbacks between deformation and melt distribution in the crust–mantle transition zone of the Oman ophiolite. *Earth Planet. Sci. Lett.* 359–360, 61–72.
- Hiraga, T., Anderson, I.M., Kohlstedt, D.L., 2004. Grain boundaries as reservoirs of incompatible elements in the Earth's mantle. *Nature (London)* 427, 699–703.
- Hirth, G., Kohlstedt, D.L., 1995. Experimental constraints on the dynamics of the partially molten upper-mantle. 2. Deformation in the dislocation creep regime. *J. Geophys. Res.—Solid Earth* 100, 15441–15449.
- Hirth, G., Kohlstedt, D.L., 2003. Rheology of the Upper Mantle and the Mantle Wedge: A View From the Experimentalists, Inside the Subduction Factory. American Geophysical Union, Washington DC, pp. 83–105.
- Jaroslowski, G.E., Hirth, G., Dick, H.J.B., 1996. Abyssal peridotite mylonites: implications for grain-size sensitive flow and strain localization in the oceanic lithosphere. *Tectonophysics* 256, 17–37.
- Jin, D., Karato, S.-i., Obata, M., 1998. Mechanisms of shear localization in the continental lithosphere; inference from the deformation microstructures of peridotites from the Ivrea Zone, northwestern Italy. In: Rutter, E.H., Boriani, A., Brodie, K.H., Burlini, L., Treagus, S.H. (Eds.), *Structures and Properties of High Strain Zones in Rocks*. Pergamon, Oxford-New York, International, pp. 195–209.
- Jung, H., Karato, S.-i., 2001. Water-induced fabric transitions in olivine. *Science* 293, 1460–1462.
- Jung, H., Katayama, I., Jiang, Z., Hiraga, I., Karato, S., 2006. Effect of water and stress on the lattice-preferred orientation of olivine. *Tectonophysics* 421, 1–22.
- Karato, S.-i., Jung, H., Katayama, I., Skemer, P., 2008. Geodynamic significance of seismic anisotropy of the upper mantle: new insights from laboratory studies. *Annu. Rev. Earth Planet. Sci.* 36, 59–95.
- Katayama, I., Jung, H., Karato, S.-i., 2004. New type of olivine fabric from deformation experiments at modest water content and low stress. *Geology (Boulder)* 32, 1045–1048.
- Kelemen, P., Dick, H., 1995. Focused melt flow and localized deformation in the upper mantle: juxtaposition of replacive dunite and ductile shear zones in the Josephine peridotite, SW Oregon. *J. Geophys. Res.* 100, 423–438.
- Kelemen, P.B., 1990. Reaction between ultramafic rock and fractionating basaltic magma. 1. Phase-relations, the origin of calc-alkaline magma series, and the formation of discordant dunite. *J. Petrol.* 31, 51–98.
- Kelemen, P.B., Hirth, G., 2007. A periodic shear-heating mechanism for intermediate-depth earthquakes in the mantle. *Nature* 446, 787–790.
- Kelemen, P.B., Hirth, G., Shimizu, N., Spiegelman, M., Dick, H.J.B., 1997. A review of melt migration processes in the adiabatically upwelling mantle beneath oceanic spreading ridges. *Philos. Trans. R. Soc. London Ser. A—Math. Phys. Eng. Sci.* 355, 283–318.
- Kelemen, P.B., Shimizu, N., Salters, V.J.M., 1995a. Extraction of mid-ocean-ridge basalt from the upwelling mantle by focused flow of melt in dunite channels. *Nature (375)*, 747–753.
- Kelemen, P.B., Whitehead, J.A., Aharonov, E., Jordahl, K.A., 1995b. Experiments on flow focusing in soluble porous-media, with applications to melt extraction from the mantle. *J. Geophys. Res.—Solid Earth* 100, 475–496.
- Kelley, K.A., Plank, T., Grove, T.L., Stolper, E.M., Newman, S., Hauri, E., 2006. Mantle melting as a function of water content beneath back-arc basins. *J. Geophys. Res.—Solid Earth* 111, B09208.
- Koga, K., Hauri, E., Hirschmann, M., Bell, D., 2003. Hydrogen concentration analyses using SIMS and FTIR; comparison and calibration for nominally anhydrous minerals. *Geochem. Geophys. Geosyst.* 4, 1019.
- Kohlstedt, D., Mackwell, S.J., 1999. Solubility and diffusion of 'water' in silicate minerals. In: Wright, K., Catlow, R. (Eds.), *Microscopic Properties and Processes in Minerals*. Kluwer Academic Publishers, Dordrecht, Netherlands, pp. 539–559.
- Kohlstedt, D.L., 2006. The role of water in high-temperature rock deformation. In: Keppeler, H., Smyth, J. (Eds.), *Water in Nominally Anhydrous Minerals*. Mineralogical Society of America, Chantilly, VA, pp. 377–396.
- Lev, E., Hager, B.H., 2008. Rayleigh–Taylor instabilities with anisotropic lithospheric viscosity. *Geophys. J. Int.* 173, 806–814.
- Linckens, J., Herwegh, M., Muntener, O., 2011. Linking temperature estimates and microstructures in deformed polymineralic mantle rocks. *Geochem. Geophys. Geosyst.* 12, Q08004.
- Loney, R.A., Himmelburg, G.R., 1976. Structure of the Vulcan Peak alpine-type peridotite, southwestern Oregon. *Geol. Soc. Am. Bull.* 87, 259–274.
- Mackwell, S.J., Kohlstedt, D.L., Paterson, M.S., 1985. The role of water in the deformation of olivine single-crystals. *J. Geophys. Res.—Solid Earth Planets* 90, 1319–1333.
- Mehl, L., Hacker, B.R., Hirth, G., Kelemen, P.B., 2003. Arc-parallel flow within the mantle wedge: evidence from the accreted Talkeetna arc, south central Alaska. *J. Geophys. Res.* 108, 2375.
- Montesi, L.G.J., Hirth, G., 2003. Grain size evolution and the rheology of ductile shear zones: from laboratory experiments to postseismic creep. *Earth Planet. Sci. Lett.* 211, 97–110.
- Montesi, L.G.J., Zuber, M.T., 2002. A unified description of localization for application to large-scale tectonics. *J. Geophys. Res.—Solid Earth* 107 2045.
- Moresi, L., Solomatov, V., 1998. Mantle convection with a brittle lithosphere: thoughts on the global tectonic styles of the Earth and Venus. *Geophys. J. Int.* 133, 669–682.
- Morgan, Z., Liang, Y., Kelemen, P., 2008. Significance of the concentration gradients associated with dunite bodies in the Josephine and Trinity ophiolites. *Geochem. Geophys. Geosyst.* 9, Q07025.
- Peslier, A.H., Luhr, J.F., 2006. Hydrogen loss from olivines in mantle xenoliths from Simcoe (USA) and Mexico: mafic alkalic magma ascent rates and water budget of the sub-continental lithosphere. *Earth Planet. Sci. Lett.* 242, 302–319.
- Paterson, M.S., 1982. The determination of hydroxyl by infrared absorption in quartz, silicate glasses and similar materials. *Bull. de Mineral.* 105, 20–29.
- Paterson, M.S., Olgaard, D.L., 2000. Rock deformation tests to large shear strains in torsion. *J. Struct. Geol.* 22, 1341–1358.
- Quick, J.E., 1982. The origin and significance of large, tabular dunite bodies in the Trinity peridotite, Northern California. *Contrib. Mineral. Petrol.* 78, 413–422.
- Ramsay, J.G., 1980. Shear zone geometry—a review. *J. Struct. Geol.* 2, 83–99.
- Recanati, A., Kurz, M.D., Warren, J.M., Curtice, J., 2012. Helium distribution in a mantle shear zone from the Josephine Peridotite. *Earth Planet. Sci. Lett.* 359–360, 162–172.
- Regenauer-Lieb, K., Yuen, D.A., 2003. Modeling shear zones in geological and planetary sciences: solid- and fluid-thermal-mechanical approaches. *Earth-Sci. Rev.* 63, 295–349.
- Regenauer-Lieb, K., Yuen, D.A., Branlund, J., 2001. The initiation of subduction: criticality by addition of water? *Science* 294, 578–580.
- Rutter, E.H., Brodie, K.H., 1988. The role of tectonic grain size reduction in the rheological stratification of the lithosphere. In: Zankl, H., Belliere, J., Prashnowsky, A. (Eds.), *Detachment and Shear*. Springer International, Berlin, Federal Republic of Germany, pp. 295–308.
- Saleeby, J.B., Harper, G.D., Snoko, A.W., Sharp, W.D., 1982. Time relations and structural-stratigraphic patterns in Ophiolite Accretion, West Central Klamath Mountains, California. *J. Geophys. Res.* 87, 3831–3848.
- Schubert, G., Yuen, D.A., 1978. Shear heating instability in earths upper mantle. *Tectonophysics* 50, 197–205.
- Shewmon, P., 1989. *Diffusion in Solids*. Minerals, Metals, and Materials Society, Warrendale, PA.
- Skemer, P., Katayama, I., Jiang, Z., Karato, S.-i., 2005. The misorientation index: development of a new method for calculating the strength of lattice-preferred orientation. *Tectonophysics* 411, 157–167.
- Skemer, P., Warren, J.M., Hirth, G., 2012. The influence of deformation history on the interpretation of seismic anisotropy. *Geochem. Geophys. Geosyst.* 13, Q03006.
- Skemer, P., Warren, J.M., Hirth, G., 2012. The influence of deformation history on the interpretation of seismic anisotropy. *Geochem. Geophys. Geosyst.* 13,

- Skemer, P., Warren, J.M., Kelemen, P.B., Hirth, G., 2010. Microstructural and rheological evolution of a mantle shear zone. *J. Petrol.* 51, 43–53.
- Spiegelman, M., Kelemen, P.B., 2003. Extreme chemical variability as a consequence of channelized melt transport. *Geochem. Geophys. Geosyst.* 4, 1055.
- Spiegelman, M., Kelemen, P.B., Aharonov, E., 2001. Causes and consequences of flow organization during melt transport: the reaction infiltration instability in compactible media. *J. Geophys. Res.—Solid Earth* 106, 2061–2077.
- Stevenson, D.J., 1989. Spontaneous small-scale melt segregation in partial melts undergoing deformation. *Geophys. Res. Lett.* 16, 1067–1070.
- Sundberg, M., Hirth, G., Kelemen, P.B., 2010. Trapped melt in the Josephine Peridotite: implications for permeability and melt extraction in the upper mantle. *J. Petrol.* 51, 185–200.
- Tackley, P.J., 1998. Self-consistent generation of tectonic plates in three-dimensional mantle convection. *Earth Planet. Sci. Lett.* 157, 9–22.
- Takei, Y., Holtzman, B.K., 2009. Viscous constitutive relations of solid–liquid composites in terms of grain boundary contiguity: 1. grain boundary diffusion control model. *J. Geophys. Res.—Solid Earth* 114, B06205.
- Tenner, T.J., Hirschmann, M.M., Withers, A.C., Hervig, R.L., 2009. Hydrogen partitioning between nominally anhydrous upper mantle minerals and melt between 3 and 5 GPa and applications to hydrous peridotite partial melting. *Chem. Geol.* 262, 42–56.
- Tommasi, A., Knoll, M., Vauchez, A., Signorelli, J., Thoraval, C., Loge, R., 2009. Structural reactivation in plate tectonics controlled by olivine crystal anisotropy. *Nat. Geosci.* 2, 422–426.
- Trompert, R., Hansen, U., 1998. Mantle convection simulations with rheologies that generate plate-like behaviour. *Nature* 395, 686–689.
- Twiss, R.J., 1977. Theory and applicability of a recrystallized grain size paleopiezometer. *Pure Appl. Geophys.* 115, 227–244.
- Vissers, R.L.M., Drury, M.R., Newman, J., Fliervoet, T.F., 1997. Mylonitic deformation in upper mantle peridotites of the North Pyrenean Zone (France): implications for strength and strain localization in the lithosphere. *Tectonophysics* 279, 303–325.
- Warren, J.M., Hirth, G., 2006. Grain size sensitive deformation mechanisms in naturally deformed peridotites. *Earth Planet. Sci. Lett.* 248, 438–450.
- Warren, J.M., Hirth, G., Kelemen, P., 2008. Evolution of lattice-preferred orientation during simple shear in the mantle. *Earth Planet. Sci. Lett.* 272, 501–512.
- Warren, J.M., E., Hauri, Pyroxenes as tracers of mantle water variations, submitted to *J. Geophys. Res.*, in review.
- Wenk, H., 1985. Preferred Orientation in Deformed Metals and Rocks: An Introduction to Modern Texture Analysis. Academic Press, Orlando.
- White, S.H., Burrows, S.E., Carreras, J., Shaw, N.D., Humphreys, F.J., 1980. On mylonites in ductile shear zones. In: Carreras, J., Cobbold, P.R., Ramsay, J.G., White, S.H. (Eds.), *Shear Zones in Rocks*. Pergamon, Oxford-New York, International, pp. 175–187.
- Yuen, D.A., Fleitout, L., Schubert, G., Froidevaux, C., 1978. Shear deformation zones along major transform faults and subducting slabs. *Geophys. J. R. Astron. Soc.* 54, 93–119.
- Zhao, Y.H., Ginsberg, S.B., Kohlstedt, D.L., 2004. Solubility of hydrogen in olivine: dependence on temperature and iron content. *Contrib. Mineral. Petrol.* 147, 155–161.
- Zimmerman, M.E., Kohlstedt, D.L., 2004. Rheological properties of partially molten lherzolite. *J. Petrol.* 45, 275–298.